J. Fluid Mech. (1967), *vol.* 27, *part* 1, *pp.* 29–48
Printed in Great Britain

Steady free convection in a porous medium heated from below

By J. W. ELDER
Department of Applied Mathematics and Theoretical Physics, Cambridge

(Received 2 March 1966)

This is an experimental and numerical study of steady free convection in a porous medium, a system dominated by a single non-linear process, the advection of heat. The paper presents results on three topics: (1) a system uniformly heated from below, for which the flow is cellular, as in the analogous Bénard–Rayleigh flows, (ii) the role of end-effects, and (iii) the role of mass discharge. Measurements of heat transfer are used to establish further the validity of the numerical scheme proposed by the author (1966*a*), while the other flows allow a more extensive study of the numerical scheme under various boundary conditions. The results are very satisfactory even though only moderately non-linear problems can be treated at present.

The main new results are as follows. For the Rayleigh-type flow, above a critical Rayleigh number of about 40, the heat transferred across the layer is proportional to the square of the temperature difference across the layer and is independent of the thermal conductivity of the medium or the depth of the layer. This result is modified when the boundary-layer thickness is comparable to the grain size of the medium. The investigation of end-effects reveals variations in horizontal wave-number and a pronounced hysteresis and suggests an alternative explanation of some observations by Malkus (1954).

1. Introduction

The main aim of this paper is a study of the application of the numerical method proposed by the author (Elder 1966*a*) to free convection in a porous medium. From the point of view of fluid mechanics, the principal interest in convection in a porous medium is that the system is non-linear solely because of the advection of heat. This is therefore one of the simplest non-linear elliptic systems.

The paper is concerned with the flow in a homogeneous horizontal slab which is heated from *below*. It is mainly in this respect that the flow differs from that of the previous study (Elder 1966*a*) in which a uniform temperature difference was maintained across a *vertical* slot filled with viscous fluid. In that case the flow is largely uni-cellular. The present case is more complex in that, as in the Bénard–Rayleigh problem, there is no motion below the critical Rayleigh number, the consequent motion is multi-cellular and is considerably affected by end-effects. It is of interest to study these effects for a flow in which there is no advection

or diffusion of vorticity especially in so far as these flows show similar behaviour to the convection of a viscous fluid, in particular one with large Prandtl number.

The above point of view has not been the original motivation for this and other studies. Ever since the original work of Darcy (1856) there have been numerous studies by hydrologists, petroleum geologists, chemical engineers, geologists and geophysicists of flow in a porous medium. Until quite recently most of these studies have been for isothermal flow (see, for example, the review by Richardson 1961), but in the last twenty years or so geophysicists and others have begun to consider the possibility that convection in a porous medium occurs within the earth. Two principal areas of interest have so far emerged. The first and better known is related to the problem of so-called geothermal or hot-spring areas. An early study was that of Einarsson (1942). The *possibility* of free convection in a porous medium uniformly heated from below, and the similarity to the Benard–Rayleigh problem, was pointed out by Horton & Rogers (1945) and Lapwood (1948). Wooding (1957 and following papers) has greatly extended these studies, Elder (1958) and Schneider (1963) have performed laboratory experiments and Donaldson (1962) has given some numerical calculations. The second, and much more speculative, possibility is that the earth's mantle behaves like a porous medium. This idea has been used in a discussion of earthquake sources by Frank (1965) and in a model of vulcanism by Elder (1966*b*). These geophysical studies have recently been reviewed by the author (1965).

The problem is formulated in § 2. The laboratory measurements of heat transfer are described in § 3 and a similar numerical investigation is given in § 4. In the previous study it was soon found that most of the difficulties arose in the application of the boundary conditions. It therefore seemed desirable to study flows produced by a variety of boundary conditions. This is largely the purpose of §§ 5 and 6, an investigation of end effects and mass discharge; followed by a discussion in § 7.

2. Formulation of the problem

Consider the steady motion of a fluid of kinematic viscosity ν, which saturates a horizontal slab of homogeneous porous material of thickness H, horizontal extent E, permeability k, and diffusivity† κ_m. Let all the walls of the slab be held at temperature T_0 except for a centrally placed portion of the base of the slab of width L held at temperature $(T_0+\Delta T)$. Making the Boussinesq approximation, that density variations are significant only in their generation of buoyancy forces, and that other fluid parameters are independent of temperature, it is readily seen by inspection of the equations of motion that the problem is specified by: the acceleration due to buoyancy $\gamma g \Delta T$, where γ is the coefficient of cubical expansion; k/ν; H/κ_m; E; L; and the acceleration due to gravity g. This last quantity must be included for problems involving mass discharge. Hence since these six

† It is important to note that $\kappa_m = K_m/\rho c$, where K_m is the thermal conductivity of the saturated medium and ρc is the thermal capacity of the fluid. We use κ, K for the thermal diffusivity and thermal conductivity of the fluid.

parameters involve only the dimensions of length and time, four dimensionless parameters are required to define the problem. A convenient set is

$$\left.\begin{aligned} A &= k\gamma g\Delta T H/\kappa_m \nu \quad \text{(Rayleigh number)},\\ B &= gHk/\kappa_m \nu \quad \text{(discharge number)},\\ e &= E/H \quad \text{and} \quad l = L/H \quad \text{(aspect ratios)}. \end{aligned}\right\} \tag{1}$$

The only point of novelty here is the parameter B, to be called the discharge number, which is a measure of the ratio of the imposed pressure forces to the viscous forces, and can arise in problems involving mass discharge.

The field variables can be conveniently made dimensionless by choosing *units* of length, temperature, pressure, velocity

$$H, \quad \Delta T, \quad \rho_0 \nu \kappa_m/k, \quad \kappa_m/H,$$

where ρ_0 is the density of the fluid at temperature T_0. For steady motion the field equations, simplified by the Boussinesq approximation, can be written with the above units in dimensionless form (Wooding 1957)

$$\nabla . \mathbf{q} = 0, \tag{2a}$$

$$0 = -\nabla p + A\theta \mathbf{k} - \mathbf{q}, \tag{2b}$$

$$\mathbf{q} . \nabla \theta = \nabla^2 \theta, \tag{2c}$$

where $\mathbf{q}$ is the velocity, p is the departure of the pressure from its value when $A = 0$, θ is the temperature, and $\mathbf{k}$ is a unit vertical vector. We note that there is no Prandtl number effect since there are no inertia forces.

In two dimensions, erecting a Cartesian co-ordinate frame $Oxyz$ so that motion is in planes $y =$ constant and z is measured vertically upwards, and introducing a stream function ψ, we have

$$\omega = A\theta_x, \tag{3a}$$

$$\nabla^2 \psi = \omega, \tag{3b}$$

$$V = \partial(\psi, \theta), \tag{3c}$$

$$\nabla^2 \theta = V, \tag{3d}$$

where ∂ is the Jacobian operator and x is the horizontal co-ordinate. Note that $\mathbf{q} = (-\psi_z, \psi_x)$ and the vorticity $\boldsymbol{\omega} = \nabla \times \mathbf{q} = -\mathbf{j}\omega$, where $\mathbf{j}$ is the unit vector parallel to the y-axis (into the paper in the diagrams shown here). The source term V is the rate of generation of temperature and is produced solely by advection. In the discussion $\partial(\psi, \theta)$ is called the advection. We note that vorticity is generated by the horizontal gradient of the buoyancy force and that there is no advection or diffusion of vorticity.

We consider two arrangements of the boundary conditions. The first is for impermeable walls for which in the two-dimensional analysis: $\psi = \theta = 0$ on the walls except that $\theta = 1$ on $|x| \leqslant \frac{1}{2}l$, $z = 0$. The second is the same except that we allow parts of the walls to be permeable. This is discussed more fully in § 6.

3. Experimental study of heat transfer

3.1. *Experimental method*

Most of the experimental work was performed in containers filled with uniform granular material. Most convenient were glass spheres of diameter 3, 5, 8, 18 mm. However, in the largest apparatus with $L = 35{\cdot}6$ cm and $E = 180$ cm expanded plastic balls (styropor) of diameter 6 mm, glued into a porous matrix, were used. In all these cases the apparatus was of circular section.

The upper surfaces of the apparatuses were hollow metal cavities through which water was circulated from a thermostatic unit which controlled T_0 to better than $\pm 0{\cdot}1$ °C. The temperature difference across the apparatus was measured with a thermocouple and a potentiometer, which could be read to a precision of $\pm 0{\cdot}01$ °C. In spite of this, absolute values of A are known only to ± 10 % largely owing to uncertainty in k.

All the apparatuses used here were heated electrically, by placing the heater resistance in a bridge so that its resistance could always be noted. The current supplied to the bridge was determined by measuring, with a potentiometer, the voltage developed across a standard resistance. Thus the power input Q could be measured to better than ± 1 %, but uncertainty in the small heat loss through the base of the apparatus makes the error in Q about ± 5 %.

A less extensive set of measurements were made in a Hele-Shaw cell. Hele-Shaw (1898) showed that in a cavity of width $b \ll H, L$ the motion is similar to that in a porous medium. Some interesting studies using a Hele-Shaw cell have been reported by Saffman & Taylor (1958) and Wooding (1960*a*). The present experiments confirm this prediction for the case of non-isothermal flows—the phenomena found here with the beds of spheres can be duplicated in a Hele-Shaw cell. Only two-dimensional motions can be investigated, but it is a simple matter to observe the motion with suspended aluminium particles.

Similar arguments to those used by Hele-Shaw can be applied to the equations for non-isothermal flow (Wooding 1960*a*). Let U be the velocity scale and δ the smallest length scale of the motion, then three conditions are necessary:

(i) $b/\delta \ll 1$,

(ii) the Reynolds number $Ub^2/\nu\delta \ll 1$,

(iii) the Peclet number $Ub^2/\kappa\delta \ll 1$.

These conditions ensure that there is negligible advection of vorticity and rapid diffusion of vorticity and heat across the flow. For the experiments described below departure from the Hele-Shaw approximation occurred when $b/\delta \gtrsim 1$.

3.2. *Heat transfer for* $l \gg 1$†

The quantity of first interest is the Nusselt number N, a dimensionless thermal conductivity defined by

$$Q = NK_m \text{ (heated area) } \Delta T/H, \tag{4}$$

† A brief description of the data of § 3 has already been given in Elder (1965).

where Q is the power transferred across the slab. Figure 1 gives data obtained: (*a*) in a medium of glass spheres, (*b*) in a Hele-Shaw cell. The accuracy of the laboratory measurements is of order $\pm 10\,\%$. Only a small portion of the laboratory data is presented here. However, it is worth remarking that no

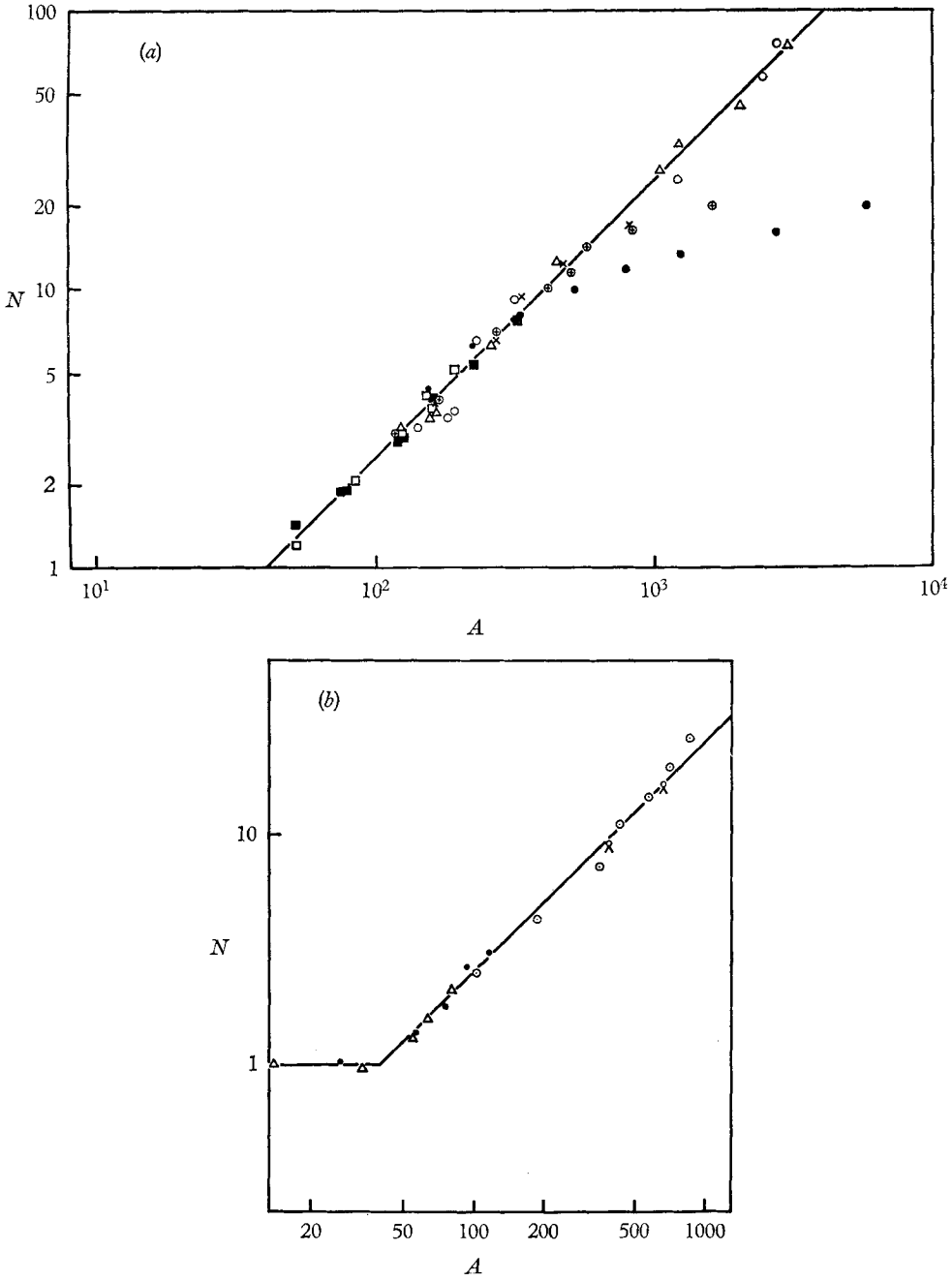

FIGURE 1. Heat-transfer characteristic $N(A)$, Nusselt number as a function of Rayleigh number: (*a*) granular material; ⊕, 8 mm spheres; ●, 18 mm spheres; (*b*) Hele-Shaw cell.

significant differences were found in $N(A)$ for media of sand, gravel, rashid rings, peas and children's marbles (the spheres of diameter 18 mm referred to in figure 1). The present results for granular material are similar to those of Schneider (1963).

3.3. *Heat transfer: quadratic region*

The heat-transfer measurements for $A \leqslant 5000$ and $l \gg 1$ are shown in figure 1. Below $A \doteqdot 40$, $N \doteqdot 1$ so that the heat transfer is entirely by conduction. Indeed, the measurements here can be used to determine K_m. At $A \doteqdot 40$ there is an abrupt change in $N(A)$; these experiments give this initial value

$$A_c = 40 \pm 10\,\%, \tag{5}$$

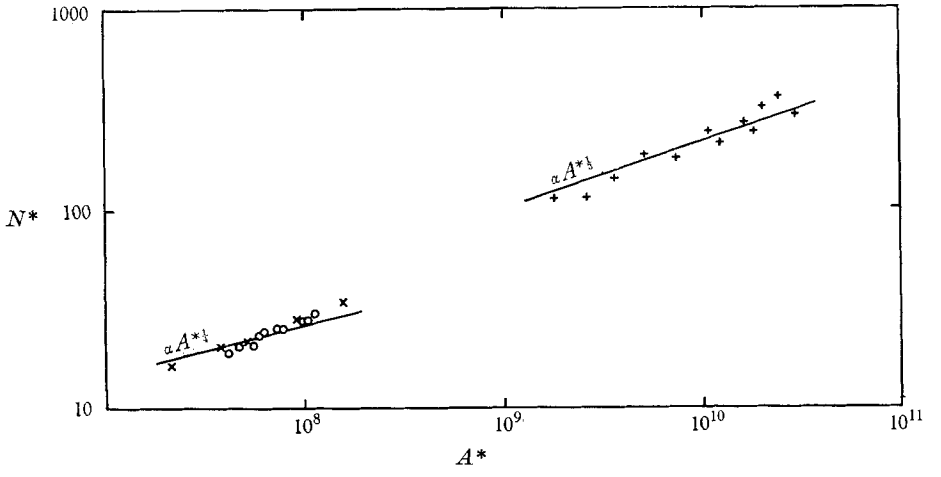

FIGURE 2. Heat-transfer characteristic $N^*(A^*)$ in the viscous-flow region with Nusselt number N^* and Rayleigh number A^* based on the fluid properties alone: +, 6 mm styropor balls, $L = H = 35{\cdot}6$ cm, diameter of slab 180 cm; ○, 3 mm styropor balls, diameter of slab 16 cm; ×, 5 mm glass spheres, $L = H = 8{\cdot}0$ cm, diameter of slab, 16 cm.

consistent with the prediction of $4\pi^2$ of Lapwood (1948). Above A_c the points lie reasonably close to

$$N = A/40 \pm 10\,\%. \tag{6}$$

In dimensional form (6) becomes

$$Q/(\text{heated area}) = k\rho c\gamma g(\Delta T)^2/40, \tag{7}$$

a quadratic relation between Q and ΔT. We note that Q is independent of H and K_m.

3.4. *Heat transfer: viscous boundary-layer region*

Above some value of the Rayleigh number, $A > A_1$ say, the experimental points begin to fall below (6). Some of these measurements are also shown in figure 1. This behaviour has also been noted by Schneider (1963). It is no longer possible to correlate the data of $N(A)$ solely by the parameters (1). Clearly an additional quantity is required. The initial departure from (6) closely follows $N \propto A^{\frac{1}{4}}$, as in simple viscous convection, suggesting the use of $A^* \equiv \gamma g \Delta T H^3/\kappa\nu$, the viscous

flow Rayleigh number. This has been done in figure 2—where N^*, A^* are now defined in terms of the parameters of the fluid alone.

The initial departure from (6) now follows

$$N^*/A^{*\frac{1}{4}} = 0{\cdot}26 \pm 0{\cdot}02, \tag{8}$$

remarkably close to the value 0·24 found by Silveston (1958) for viscous laminar convection between horizontal planes. At much higher values of A^* the curve follows

$$N^*/A^{*\frac{1}{3}} = 0{\cdot}1 \pm 0{\cdot}02 \tag{9}$$

again reasonably close to the viscous flow value of 0·06 given by Jakob (1949). The data for (9) were obtained with $L = 35{\cdot}6$ cm and 6 mm plastic balls as the medium.

Assuming both (6), (8) valid at A_1 we have

$$A_1 \doteqdot 20(H^2/k)^{\frac{1}{3}}/\xi, \tag{10}$$

where $\xi = \kappa_m/\kappa$. Writing at A_1 the Nusselt number $N_1 = H/2\delta_1$, we find typically in these experiments $\delta_1/\Delta \doteqdot 0{\cdot}2$, where Δ is the diameter of the spheres. It is not surprising that relations of the form (8) and (9) occur when the boundary-layer thickness is somewhat smaller than the scale of the porous medium. As noted by Wooding (1958) it is to be expected that equations (2) are no longer valid within a distance of order Δ from a boundary—indeed this is implicit in the definition of $\mathbf{q}$.

Here the relations (8), (9) are merely an inconvenience in so far as they limit the range of A accessible to a given apparatus. However, in the problem of convection in the earth's mantle, assuming that the mantle behaves like a porous medium, the change from porous to viscous flow may be of importance in describing the region between the lower and upper mantle.

4. Numerical study of heat transfer

4.1. *Numerical method*

A suitable finite difference representation of (3) is readily found by well-known methods (Fox 1962). The equations are solved as written in (3) in the order $(a, b, c, d, a, \ldots)$ until the solution has converged or the calculation is terminated when the solution begins to diverge. The solution of the Poisson equations (3*b*), (3*d*) is very straightforward since both $\psi\,(=0)$ and θ are given on the boundary. Leibmann's extrapolated method with alternating directions of scan is used. These matters are discussed elsewhere (Elder 1966*a*).

Most of the solutions are for a mesh spacing of order 1/20 for which the accuracy is of order 1 %. Solutions are generally terminated when values over the mesh change by less than 0·1 %.

4.2. *Convergence of the solutions*

The convergence of the solutions is indicated in figure 3 (obtained during the solutions for figures 4, 5). A parameter typical of the temperature field, the Nusselt number, is plotted against the number of scans of (3) for various Rayleigh

numbers. It is seen that the rate of convergence is more rapid at higher values of A and that for $A \gtrsim 80$ there is some overshoot. At Rayleigh numbers near the critical value of $4\pi^2$ (Lapwood 1948) the convergence is extremely slow. It is of interest to comment on this observation.

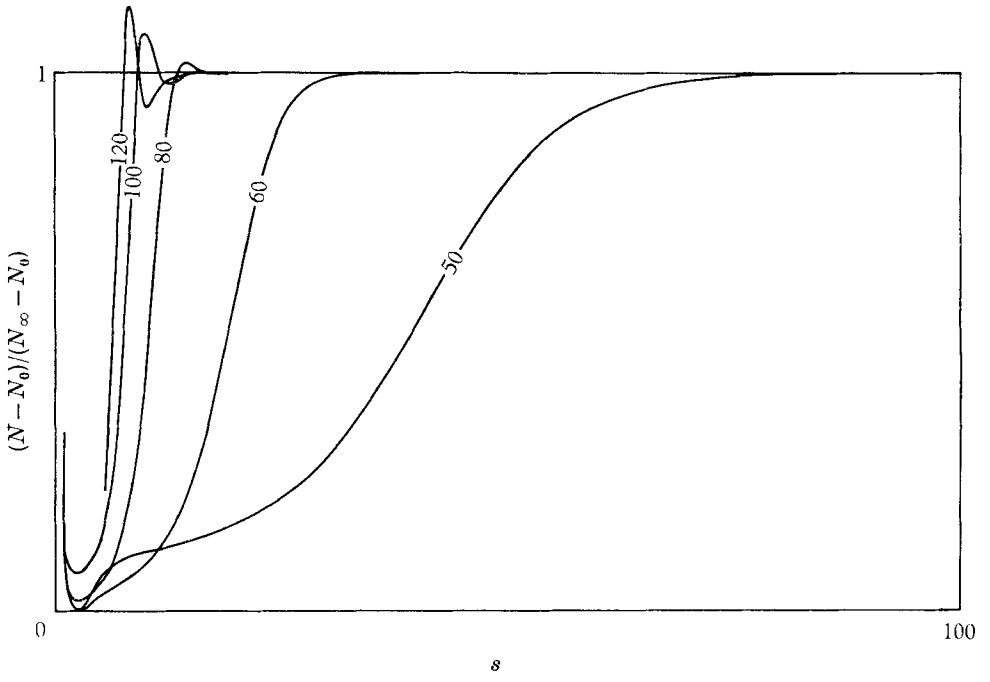

FIGURE 3. Convergence of the numerical solution for $l \gg 1$. Nusselt number N as a function of the number of scans s at various Rayleigh numbers A. Values scaled using $N_0 = 1$ and the final value N_∞. Mesh 21×21.

As Garabedian (1956) has pointed out, the solution of an iterative procedure, such as that used here, converges in a manner similar to that of the corresponding time-dependent problem at large times. We may obtain a rather crude estimate of the relation between the number of scans s and the time t by solving (3) with the same initial conditions (θ and $\psi = 0$ everywhere except for $\theta = 1$ on $z = 0$) at $A = 0$. We find that the final solution is approached exponentially so that, for example, if N is the Nusselt number, $N_\infty - N \sim e^{-s/\tau}$ and $\tau \propto d^{-2}$. For the data of figure 3 with $d = 1/20$ we find $\tau = 2{\cdot}0$ scans so that $\tau \doteqdot 0{\cdot}005 d^{-2}$ scans. From the theory of heat conduction (Carslaw & Jaeger 1959, § 3.4) we obtain a similar result with a time constant $1/\pi^2$. Hence, from the data of figure 3 we can relate the number of scans s to the dimensionless time t by

$$t \sim (200 d^2/\pi^2)\, s. \tag{11}$$

We note the important result that as the critical Rayleigh number is approached (from above) the time for the establishment of the steady motion is considerably larger than the time to heat the slab solely by conduction. For example, at $A = 50$, as shown in figure 3, the solution has converged by $s \approx 80$

when, from (11), $t \approx 40/\pi^2$, corresponding to a rate 40 times slower than that of conduction alone. For this reason attempts to study the instability of a layer of fluid suddenly heated from below, by the assumption that the temperature field is quasi-steady, are bound to fail (Foster 1965).

4.3. *Heat transfer: quadratic region*

The Nusselt number has been evaluated for some of the numerical solutions. These values are given in table 1. They show, within the numerical accuracy, for $A > 40$ that approximately $N \propto A$. The values are in excellent agreement with the laboratory values.

A	$1/d = 10$	15	20	25	30	40	∞	$100N_\infty/A$
45	—	—	—	(1·09)	—	—	1·20	2·66
50	> 1·01	1·19	1·26	1·30	—	—	1·36	2·73
60	1·36	1·51	1·58	1·62	1·64	—	1·70	2·83
70	—	—	—	1·87	1·90	—	1·92	2·75
80	1·80	1·96	2·04	2·08	2·12	—	2·02	2·52
90	—	—	—	2·27	2·30	—	2·33	2·58
100	2·09	2·28	2·37	(2·42)	2·46	2·51	2·62	2·62

TABLE 1. Numerical values of the Nusselt number $N(A, d)$ in a square box with mesh spacing d and Rayleigh number A. The values $d = \infty$ are obtained assuming $N_\infty - N \sim d^2$, and are estimated to about $\pm 2\%$. The values in brackets are for $1/d = 24$. (PM 1-32.)

4.4. *The flow field for $l \gg 1$*

When $l \gg 1$, the flow field has either no motion or is composed of cells. This cellular régime is predicted by the linear theory and confirmed both in the laboratory and numerically.

Figure 4 shows the temperature distribution† in a half-cell for $l \gg 1$ at various Rayleigh numbers, obtained numerically. Below $A \doteqdot 40$, $\psi = 0$ and $\theta = 1 - z$. The numerical solution is very stable; any disturbance decays rapidly. As A increases beyond 40 the isotherms steepen till mushroom-like distributions are produced. This feature has already been pointed out by Wooding (1957), Elder (1958) and Donaldson (1962).

Figure 5 shows the stream function and the advection at $A = 120$. The form of the stream function is not greatly different from its value near A_c except that it is a little twisted. For $l \to \infty$ with equations (2), it is readily seen that the phase of the cellular motion is theoretically indeterminate. Both in the laboratory and numerically it is found that if $l \gg 1$ but finite the phase is determined by the motion in the ends of the slab (see §§ 5.1, 5.3).

4.5. *Discussion of the heat transfer data*

A result of the form (6) is to be expected. When $A \gg A_c$ so that there is a boundary layer on $z = 0$, we have by (4) that $N \sim 1/\delta$ where δ is a measure of the boundary-layer thickness. But if W is a vertical velocity scale typical of the layer it follows

† Note: in these figures the vertical scale is 5/3 of the horizontal scale.

from (2*c*), assuming $\theta_{zz} \gg \theta_{xx}$, that $W \sim 1/\delta$. Finally, we note from the z-component of (2*b*) that $W \sim A$. Hence we expect $N \sim A$. This result, therefore, implies that there is a balance between buoyancy forces and viscous forces and that while the heat enters the slab by conduction it is carried away from the immediate vicinity of the heated surface by vertical advection which is dominant in the outer portion of the boundary layer on the heated surface.

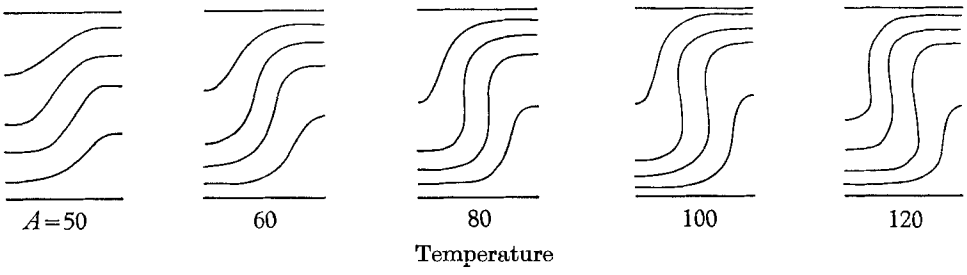

FIGURE 4. Temperature distribution in a half-cell calculated at Rayleigh number A = 50, 60, 80, 100, 120. Isotherms drawn at intervals 0(0·2)1. Mesh 21 × 21.

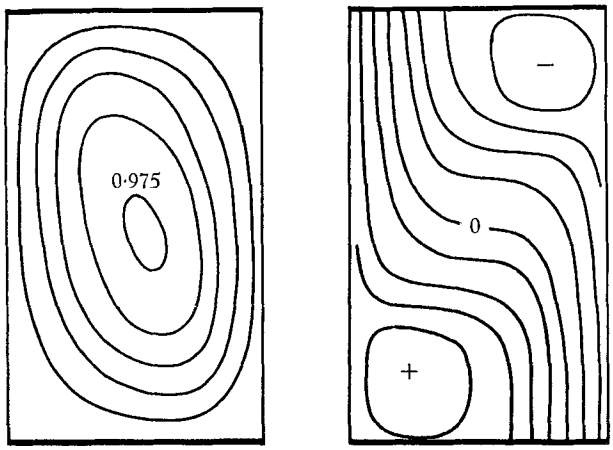

FIGURE 5. Stream function and advection in a half-cell calculated at Rayleigh number A = 120. Contours drawn at intervals of −1(0·2)1 of the maximum absolute value (indicated below the figure). Mesh 21 × 21.

The consistency of both the experimental and the numerical data in the quadratic region of the empirical expression (6) confirms the experimental procedure, the validity of the Hele-Shaw cell approximation for non-isothermal flows and the numerical method. We may therefore proceed using the numerical method with some confidence. Our interest now will concentrate on the role of different boundary conditions from those used above. While our immediate objective is to test the numerical scheme under diverse boundary conditions the flows are of considerable interest in themselves.

5. End-effects

In spite of the numerous studies of free convection, it is surprising to note that there has been relatively little consideration of end-effects, viz. for the present problem the peculiarities which arise when the aspect ratios l and e are finite.

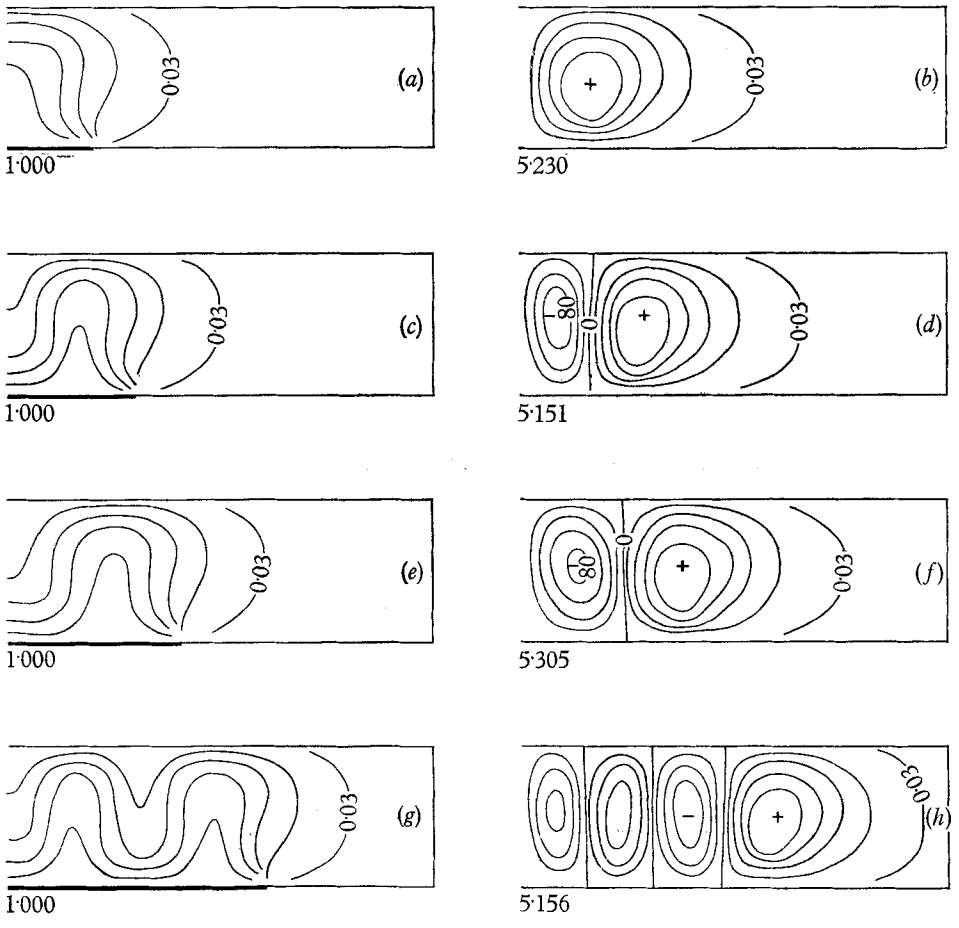

FIGURE 6. End-effects. Isotherms and streamlines in a slab of horizontal extent $e = 10$ calculated at Rayleigh number $A = 80$, mesh spacing $d = \frac{1}{15}$ and various values of the heater length l; (*a*) and (*b*), $l = 2$; (*c*) and (*d*), $l = 3$; (*e*) and (*f*), $l = 4$; (*g*) and (*h*) $l = 6$. Apart from the contour 0·03, the contours are at intervals $-1(0{\cdot}2)1$ of the maximum value of the function.

There is a great variety of end-effects in free convection. Some of the author's experiments were reported at the 1963 British Theoretical Mechanics conference at Liverpool when his attention was directed to somewhat similar phenomena in Couette flow being studied by Coles (1965). To take an analogy from atomic physics, the end-effects tend to remove a degeneracy of the system. Much work remains in this subject but the present results are of some interest.

5.1. *Numerical experiments on a simple end-effect*

The numerical solution for a flow in a slab of horizontal extent $e = 10$ for $l = 2, 3, 4$, and 6 at $A = 80$ are shown in figure 6. Only the right-hand half of the flow is shown.

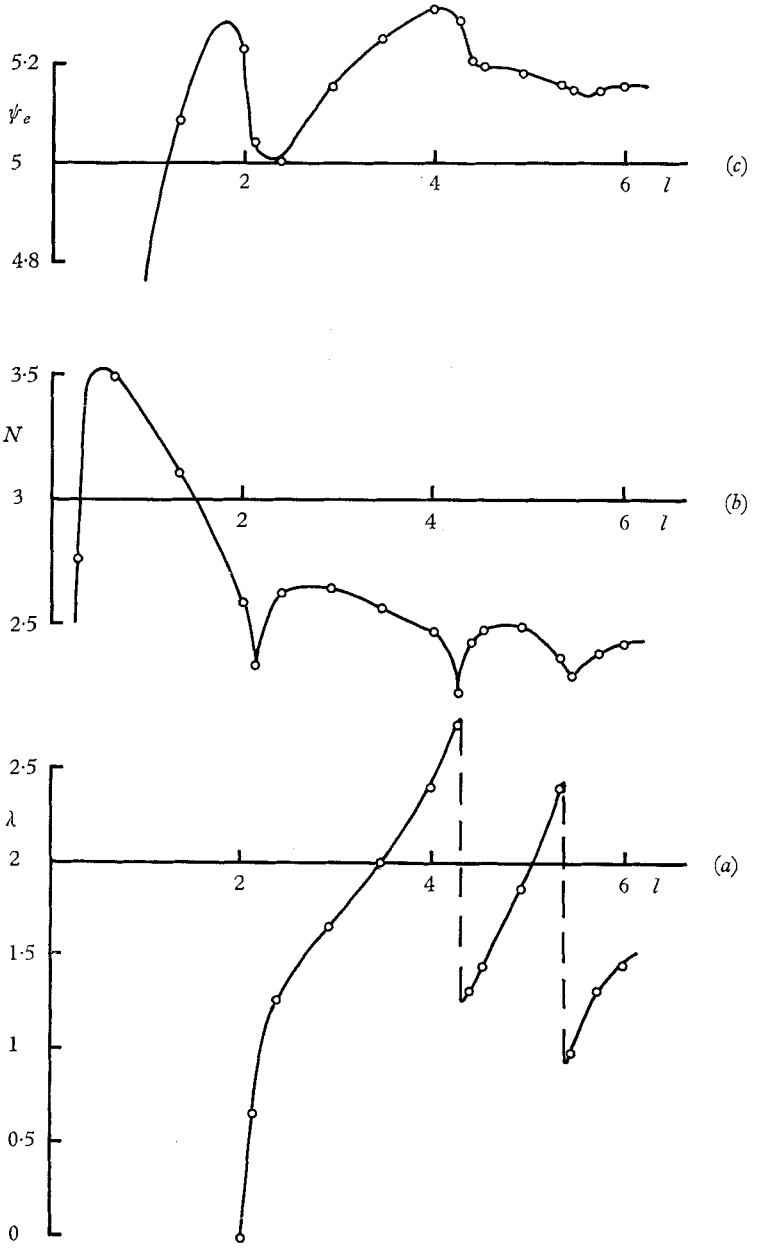

FIGURE 7. End-effects, role of heater length l on: (*a*) wavelength λ of inner Rayleigh cell; (*b*) Nusselt number N; (*c*) maximum value of the streamfunction ψ_e (of the end cells). Parameters as in figure 6. (PM 47–65.)

For $l = 2$, figures 6(*a*) and (*b*), there are two regions of opposite circulation. These *end cells* give a fairly narrow column of heated fluid rising above the heated region with a more diffuse return flow in the outer portion of the slab. We note that the flow distant from the heater, near the vertical walls, is very weak. However, for $l > 2$ in addition to the end cells there are nearly square cells, occurring in pairs of opposite circulation, above the central portion of the heated surface. We shall call these *Rayleigh cells*. For $l = 3$, figures 6(*c*) and (*d*), there is one pair of Rayleigh cells. Incidentally, we note that the flow on $x = 0$ is downward. Clearly the phase of the Rayleigh cells is set by their number and the phase of the end cells, which is always as in figure 6(*b*). In figures 6(*e*) and (*f*) with $l = 4$, the motion is as for $l = 3$ except that the Rayleigh cells have a much larger wavelength. For $l = 6$, figures 6(*g*) and (*h*), three pairs of Rayleigh cells appear.

The gross changes of the system as l is varied are summarized in figure 7 which shows: the wavelength λ of the inner pair of Rayleigh cells for the same arrangement used in figure 6; the Nusselt number N; and the maximum value of the streamfunction ψ_e, which in fact corresponds to that of the end cells.

The breaks in the curves correspond to the appearance of pairs of Rayleigh cells at $l = 2{\cdot}0,\ 4{\cdot}3,\ 5{\cdot}4$. The changes in wavelength are closely paralleled by corresponding changes in N and ψ_e.

5.2. *Linear analysis of the simple end-effect*

A partial understanding of the above phenomena is possible with an analysis similar to that used by Zierep (1961) for the corresponding problem with a viscous fluid.

As $A \to 0$, $\psi \to 0$ and $\nabla^2\theta \to 0$, so that we write the temperature field as $\theta = \beta(1-z)$; where $\beta = 1$ for $|x| \leqslant \frac{1}{2}l$ to be called region 1 and $\beta = 0$ for $|x| > \frac{1}{2}l$, to be called region 2. This is a rather crude representation of θ but sufficient for the moment. Consider a steady perturbation (θ', ψ') superimposed on this state of rest. Retaining only first-order quantities

$$\{\nabla^4 + \beta A(\partial^2/\partial x^2)\}(\theta', \psi') = 0, \tag{12}$$

where $(\theta', \psi') = 0$ on $z = 0, 1$.

The field is assumed symmetrical about $x = 0$, so we refer only to the region $x \geqslant 0$. Suitable solutions for regions 1, 2 are

$$\theta'_1 = a \cos m\pi x \sin n\pi z, \tag{13a}$$

$$\theta'_2 = a \cos \tfrac{1}{2}m\pi l\, e^{-\pi(x-\frac{1}{2}l)} \sin n\pi z, \tag{13b}$$

where $n = 1, 2, 3, \ldots$, a is an arbitrary constant and we have placed $\theta'_1 = \theta'_2$ on $x = \frac{1}{2}l$. Note that, when l is an odd integer and $m = 1$, $\theta'_2 = 0$. This feature arises from the approximation to the original temperature field. These are solutions of (12) provided

$$A = \pi^2(m^2 + n^2)^2/m^2. \tag{14}$$

A has a minimum value when $m = n$ of $4\pi^2 n^2$. The first occasion when this is possible is when $n = 1$. Hence only for $A \geqslant 4\pi^2$ is the above solution possible. For $l = \infty$, $4\pi^2$ is the critical Rayleigh number A_c (Lapwood 1948). For l finite and $A < 4\pi^2$ the complex roots for m must be used. Here we simply consider the

situation $A = 4\pi^2$, $m = n = 1$. It is seen that square cells appear in $|x| < \frac{1}{2}l$ for $l \geqslant 2$; with $l < 2$ there is merely a single column of rising heated fluid. The end cells decay exponentially in the lateral direction.

This analysis suggests that successive pairs of Rayleigh cells will appear when $l = 2, 4, 6, \ldots$. In the numerical calculations of § 5.1 we found these values to be $l = 2{\cdot}0, 4{\cdot}3, 5{\cdot}4$ at $A = 80$. The flow at $A = 80$ cannot be expected to satisfy the linear theory, yet the progression of events is moderately well described.

A very crude discussion of the variation of the Nusselt number as a function of l and e is now possible. Let us assume as in (6) that each Rayleigh cell transfers an amount of heat corresponding to a Nusselt number of αA and each end cell an amount $\alpha' A$, where α is a constant and α' is independent of A. Then, if we write $l = 2(c+r)$ where r is an integer, r is the number of half Rayleigh cells and c the length of the heated boundary accessible to an end cell. Hence the total Nusselt number is $2(c\alpha' + r\alpha)$. We try various guesses for the form of α'. If $\alpha' = \text{const.}$, the curve $N(l/e)$ continuously rises between the breaks which occur when r increases by unity, contrary to the data of figure 7 (*b*). If $\alpha' \propto 1/c$ the curve similarly falls. A crude compromise is $\alpha' = \alpha/c^{\frac{1}{2}}$, where we choose for want of a better assumption $\alpha' = \alpha$ when $c = 1$. This leads to a curve roughly similar to that of figure 7 (*b*) but with the breaks at $r = 2, 4, 6, \ldots$. The principal oversimplification of the above discussion is its neglect of the interaction between the end cells and the Rayleigh cells, clearly shown in the data of figures 6 and 7 and especially in the experiment of the following section. Nevertheless, the general form of the relation $N(l, e)$ is indicated. Finally, we note therefore that the rapid fall in N for $l \lesssim 0{\cdot}5$ shown in figure 7 (*b*) is probably a finite difference effect, viz. that the heater is represented by too few mesh points.

5.3. *Hysteresis*

One of the most interesting effects in the experiments with the Hele-Shaw cell is found with l finite but in which the horizontal extent of the slab is very much larger than l. Figure 8, plate 1, is a photographic sequence of the flow revealed with suspended aluminium powder. Each of these flows has been left for sufficient time for it to come into a steady state. Figure 8 (*a*) shows a regular group of nearly square cells above the heated surface with weaker circulations in the end regions. The motion is quite steady. In figure 8 (*b*) at a somewhat higher Rayleigh number the distribution and width of the cells is rather irregular. The motion is very slowly but continually changing. We note the growth of the cells in the end regions. This process continues in figures 8 (*c*), (*d*). In figure 8 (*d*) the inner cells are again nearly square and the motion is nearly as steady as in figure 8 (*a*). In figures 8 (*e*), (*f*) the process continues. It is seen that the progressive change in the flow is dominated by the growth and encroachment of the cells in the end region. In general there are an even number of Rayleigh cells and the motion is steadiest when the Rayleigh cells are square.

The motion of figure 8 (*f*) persists to large Rayleigh numbers. On the other hand, if the Rayleigh number is now very slowly reduced, the motion of figure 8 (*f*) persists to Rayleigh numbers about that of figure 8 (*a*). The first reappearance is shown in figure 8 (*g*). Here we have a pronounced hysteresis. It follows that to specify the thermodynamic state of the system the path by which that state was

achieved should also be specified. A somewhat similar hysteresis, although more complex, has been observed by Coles (1965) for the flow between concentric rotating cylinders.

5.4. *A comment on an experiment by Malkus*

It is possible that this phenomenon of the appearance of end-effects and in particular the variation in horizontal wave-number provides an alternative explanation to that given by Malkus (1954) for his measurements of 'transitions' in convection in a viscous fluid.

Malkus has reported, in his experiment to determine the relation between the heat transfer and the Rayleigh number for a horizontal layer of a viscous fluid, that there were discontinuous changes in the slope of the curve. He has interpreted these changes as due to the progressive appearance of higher modes of the linear stability analysis. That is, changes occur when the Rayleigh number is sufficiently high for the vertical wave-number to have values $\pi, 2\pi, 3\pi, \ldots$.

It has not been realized hitherto that an alternative possibility could be the availability of additional horizontal wave-numbers. Some experiments by the author for the Rayleigh–Bénard problem also reveal pronounced end-effects. I have not, however, been able to reproduce the rather small changes of slope in $N(A)$ found by Malkus. These experiments are to be reported.

6. Mass discharge

A problem of particular interest to the geophysicist for studies of both hydrothermal systems and penetrative convection in the upper mantle is the flow when it is dominated by mass discharge. The laboratory experiments and their relation to hydrothermal systems have already been described (Elder 1965); here we shall discuss the numerical experiments.

Our particular interest, keeping in mind other possible applications of the numerical procedure, is to show that the method used below is satisfactory in dealing with the boundary conditions which arise with mass discharge in a convective system.

Two extreme possibilities arise: forced and natural discharge. In forced discharge we consider that the discharge arises from the ambient pressure field, e.g. due to variations of the water-table level. In natural discharge we consider that the ambient variations of the pressure are negligible; the discharge is driven solely by the pressure field arising from the differential heating of the fluid.

6.1. *Forced discharge*

Figure 9 shows the results of a calculation with forced discharge. The vertical velocity ψ_x has been specified on $z = 1$, to be finite on $|x| \leqslant \frac{1}{2}$ and elsewhere to be zero, and the velocity has been required to be horizontal on the vertical ends of the slab. The flow field for $A = 0$, obtained from $\nabla^2\psi = 0$, is also shown in figure 9, together with the flow field when there is no discharge. The motion when there is both discharge and convection can be regarded as a non-linear interaction of these two fields. The discharge aids the motion in the end regions so that

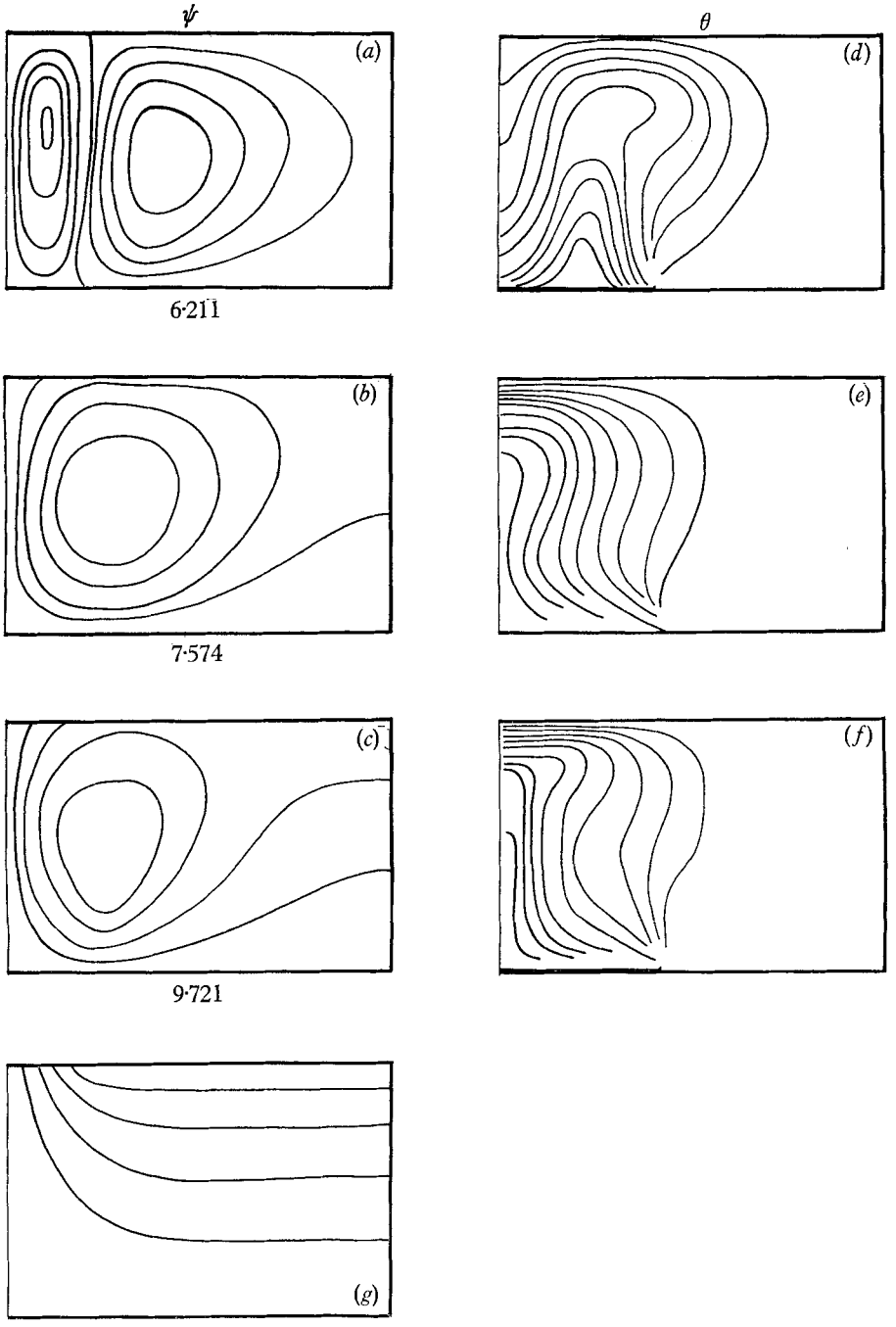

FIGURE 9. Forced discharge, calculated distributions of temperature and stream function. Discharge over zone of width 1. $A = 100$, $l = 2$, $e = 5$, 101×21 mesh. Only the right half of the flow is shown. (*a*) and (*d*) no discharge; (*b*) and (*e*) discharge velocity 2·5; (*c*) and (*f*) discharge velocity 5·0; (*g*) $A = 0$ with discharge. (POR 36.)

the ordinary cellular mode is annihilated with the discharge used here. An important feature (Elder 1965) of the flow is that even at quite large discharge rates some of the fluid is recirculated even though, when the discharge velocity is 5 as in figure 6(*c*), the problem is essentially one of forced convection.

6.2. *Natural discharge*

For a natural discharge we assume that the pressure p is maintained at zero on $z = 1$. Physically this implies that any fluid which passes above $z = 1$ is allowed to run away and is lost to the system. Here the return flow is also allowed to enter only on $z = 1$. The calculations proceed thus. After each scan of (3) we solve

$$\nabla^2 p = A\theta_z, \tag{15}$$

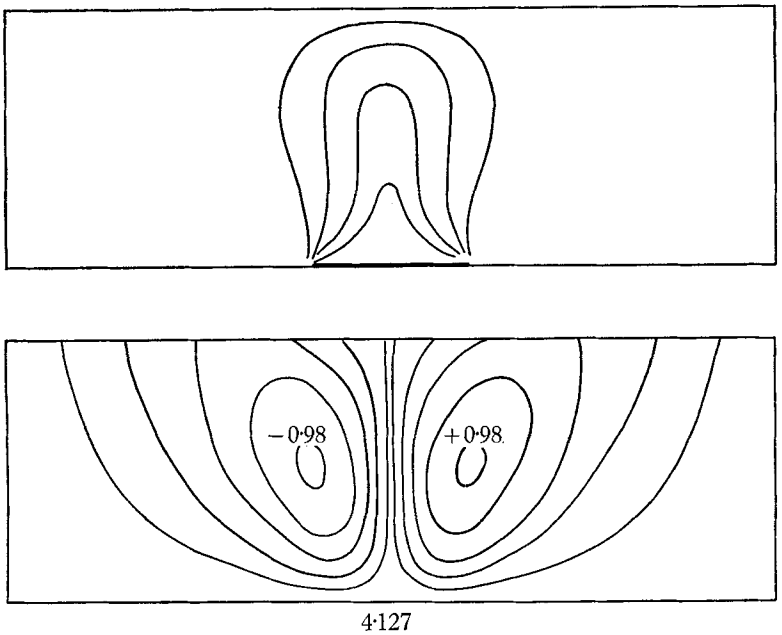

4·127

FIGURE 10. Natural discharge, calculated isotherms (above) and stream function. $A = 50$, $l = 1$, $e = 5$, mesh 101×21. (POR 67.)

which follow from (2*a*) and (2*b*). Since on $z = 1$ we require $p = 0$ and $\theta = 0$, from (2*b*) the surface vertical velocity $\psi_x = -p_z$. In the calculation we therefore, at the end of each scan, simply impose the stream function on $z = 1$ to be

$$\psi(x, 1) = -\int_0^x p_z(x, 1)\, dx, \tag{16}$$

where in (16) p is the solution of (15). This has proved to be a satisfactory scheme although somewhat slower than the simple scheme (3).

Figure 10 shows the temperature and stream function distributions for a Rayleigh number $A = 50$. Recharge occurs over the bulk of the upper surface, the heated fluid rises as a fairly thin column even at this rather low Rayleigh number, and only about 30 % of the fluid in the plume is recirculated. In natural

systems with very large Rayleigh numbers we anticipate that only a very small portion of fluid is recirculated.

Figure 11 shows two characteristic parameters of the flow. Figure 11 (*a*) shows the local Nusselt number $N' = N'(x)$ on $z = 0$ and $z = 1$. The pronounced discontinuity at the ends of the heated surface is simply a feature of our boundary conditions. What is of considerable geophysical interest is that the heat flux on $z = 1$ falls rapidly to zero outside the region of the discharge. Figure 11 (*b*) shows the discharge velocity. Discharge occurs over a region of width 1·4; elsewhere the flow is into the slab. This inward flow is sufficient to reduce the surface heat flux to zero.

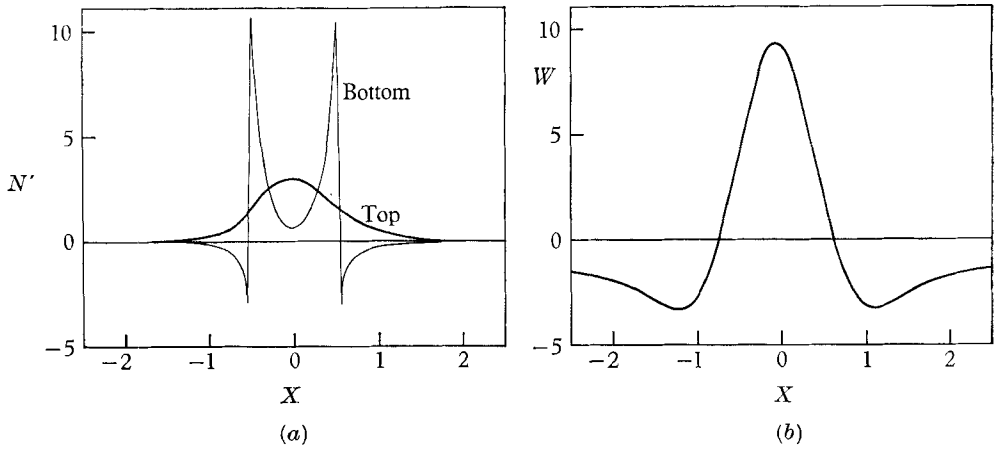

FIGURE 11. Natural discharge, parameters as in figure 10. (*a*) Heat flux N'; (*b*) velocity through the upper surface W.

In the Hele-Shaw cell the natural discharge is simply arranged by having a small gap in the lid (through which the coolant is circulated) leading into an upper wide chamber full of fluid. Figure 12, plate 2, is a photograph of such a flow. It should be compared with figure 10. Even though it is at a much higher Rayleigh number, the gross features, including the recirculation, are similar to the numerical solution.

The solution to the linearized problem, following Lapwood (1948), is obtained simply by requiring $n = \frac{1}{2}, \frac{3}{2}, \ldots$ in (13) so that $p = 0$ on $z = 1$. Motion is first possible with $n = \frac{1}{2}$ and the corresponding critical Rayleigh number of π^2. Otherwise there is no novelty in this solution. However, at Rayleigh numbers much greater than critical the motion is seen to be dominated by a boundary layer on the heated surface and a plume rising above it. Wooding (1963) has given a most revealing analysis of the flow in the plume when the flow is sufficiently dominated by the discharge that there is minor recirculation of fluid; i.e. fluid particles make only a single pass through the system. Since in the fluid surrounding the plume $p = 0$, if the plume is sufficiently thin, to the order of the boundary-layer approximation, $p = 0$ everywhere and hence, by (2*b*), $W = A\theta$. This relation implies a balance between viscous and buoyancy forces.

7. Concluding remarks

Some of the above flows are crudely analogous to the corresponding flows of a viscous fluid. This is particularly the case when inertial effects, which arise with a viscous fluid, are small, either because the Prandtl number is large or because, near the critical Rayleigh number, the advection of vorticity is negligible. There is the important difference, however, that flow in a porous medium provides a realization of so-called free–free boundary conditions, whereas, while frequently used in a preliminary analysis, these are rather artificial boundary conditions for a viscous fluid.

Near the critical Rayleigh number, the flows are very similar, as pointed out in the analyses of Horton & Rogers (1945) and Lapwood (1948). The essential difference is that, while in both cases inertial effects are negligible, we must allow for diffusion of vorticity in a viscous fluid. This merely changes the operator ∇^4 in (12) to ∇^6, an increase by a factor of $\pi^2(m^2+n^2)$. Consequently the critical Rayleigh number is increased from $4\pi^2$ to $27\pi^4/4$ and the width of the cells by $\sqrt{2}$ (Chandrasekhar 1961).

Above the critical Rayleigh number, (6) suggests that $N \doteq A/A_c$, so that we might anticipate a similar relation in a viscous fluid. Inspection of Silveston's (1958) measurements shows that indeed $N^* \doteq A^*/A_c^*$ up to $N^* \approx 1{\cdot}5$, suggesting that inertial effects are negligible here. Beyond this value, however, the experimental curve falls rapidly below the linear relation. This is undoubtedly due to the rapid increase in the advection of vorticity and the growth of viscous boundary layers. Nevertheless, both flows are cellular and strongly influenced by end-effects. A study of end-effects for free convection of a viscous fluid will be reported elsewhere. It is sufficient here to note that as with flow in a porous medium the phase of the cellular motion, the distribution of horizontal wavenumbers, and hysteresis are dominated by the end cells.

The laboratory experiments referred to in § 3 were done at Geophysics Division, Department of Scientific and Industrial Research, Wellington, New Zealand. I am very grateful for the assistance of Mr W. J. P. MacDonald. The numerical study was supported by National Science Foundation Grant GP-2414 and Office of Naval Research Contract Nonr-2216 while I was at the Institute of Geophysics and Planetary Physics, La Jolla. The numerical work was done on the CDC 3600 computer at the University of California, San Diego computing centre. The manuscript was written while I was supported by a grant from the British Admiralty.

REFERENCES

CARSLAW, H. S. & JAEGER, J. C. 1959 *Conduction of Heat in Solids*. Oxford: Clarendon Press.

CHANDRASEKHAR, S. 1961 *Hydrodynamic and Hydromagnetic Stability*. Oxford: Clarendon Press.

COLES, D. 1965 *J. Fluid Mech.* **21**, 385.

DARCY, H. P. G. 1856 *Les Fontaines publiques de la ville de Dijon*. Paris: Victor Dalmont.

DONALDSON, I. G. 1962 *J. Geophys. Res.* **67**, 3449.

EINARSSON, T. 1942 *Rit. Visind. Isl.* **26**, 1.

ELDER, J. W. 1958 Ph.D. Thesis, Cambridge.

ELDER, J. W. 1965 Terrestrial Heat Flow, chap. 8. (Ed. W. H. K. Lee.) *Amer. Geophys. U. Monograph*, no. 8.

ELDER, J. W. 1966*a* *J. Fluid Mech.* **24**, 823.

ELDER, J. W. 1966*b* *Bull. Volcan.* **29** (in the Press).

FOSTER, T. D. 1965 Personal communication, to be published.

FOX, L. 1962 *Numerical Solution of Ordinary and Partial Differential Equations.* London: Pergamon Press.

FRANK, F. C. 1965 *Rev. Geophys.* **3**, 485.

GARABEDIAN, P. R. 1956 *Math. Tables Aids Comput.* **10**, 183.

HELE-SHAW, H. S. J. 1898 *Trans. Inst. Nav. Arch.* **40**, 21.

HORTON, C. W. & ROGERS, F. T. 1945 *J. Applied Phys.* **16**, 367. (See also **22**, 1476.)

JAKOB, M. 1949 *Heat Transfer.* New York: Wiley.

LAPWOOD, E. R. 1948 *Proc. Camb. Phil. Soc.* **44**, 508.

MALKUS, W. V. R. 1954 *Proc. Roy. Soc.* A **225**, 185.

RICHARDSON, J. G. 1961 *Handbook of Fluid Dynamics*, sec. 16 (ed. V. L. Streeter). New York: McGraw-Hill.

SAFFMAN, P. G. & TAYLOR, G. I. 1958 *Proc. Roy. Soc.* A **245**, 312.

SCHNEIDER, K. J. 1963 11th Int. Cong. of Refrigeration, paper 11–4, Munich.

SILVESTON, P. L. 1958 *Forsch. Ing.* **24**, 29.

WOODING, R. A. 1957 *J. Fluid Mech.* **2**, 273.

WOODING, R. A. 1958 *J. Fluid Mech.* **3**, 582.

WOODING, R. A. 1959 *Proc. Roy. Soc.* A **252**, 120.

WOODING, R. A. 1960*a* *J. Fluid Mech.* **7**, 501.

WOODING, R. A. 1960*b* *J. Fluid Mech.* **9**, 183.

WOODING, R. A. 1962 *J. Fluid Mech.* **13**, 129.

WOODING, R. A. 1963 *J. Fluid Mech.* **15**, 527.

ZIEREP, J. 1961 *ZAMM.* **41**, 114.

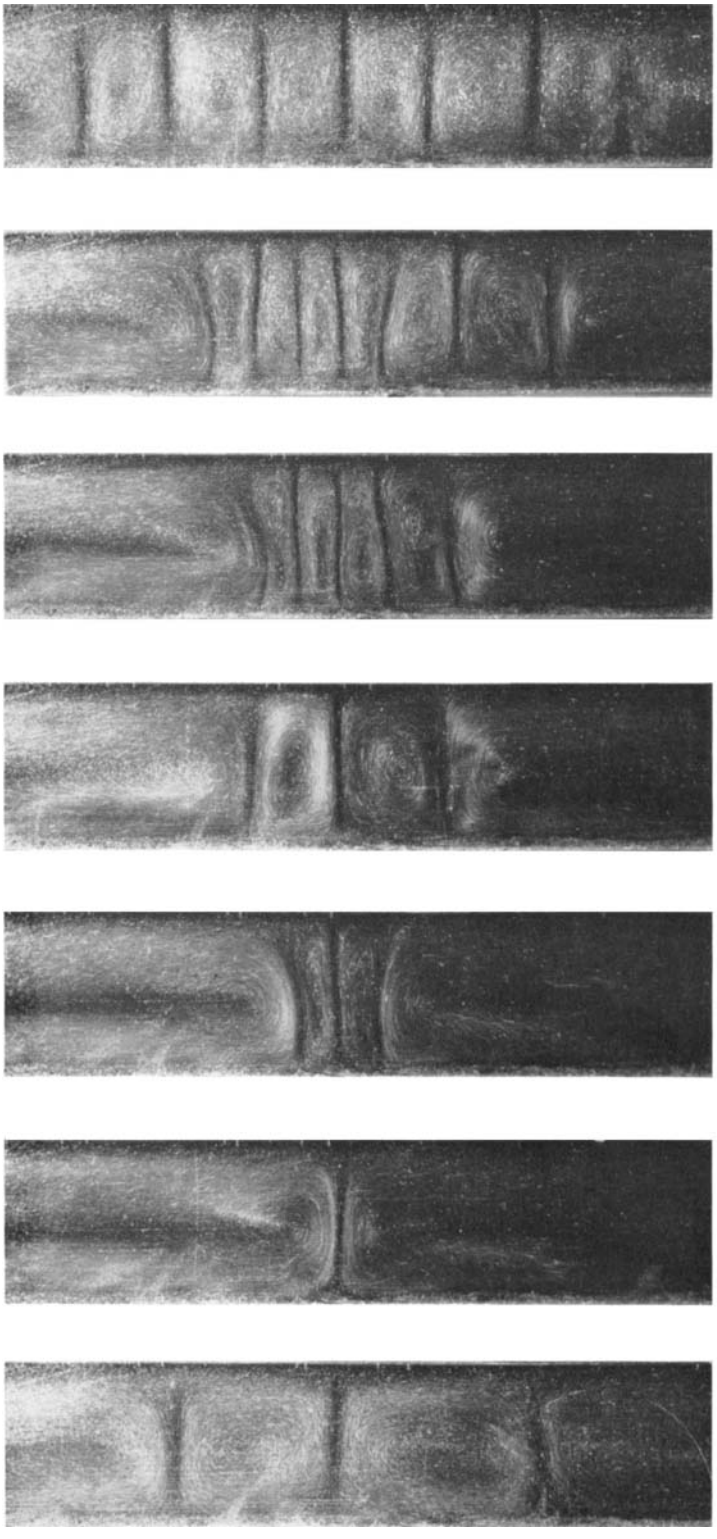

FIGURE 8. End-effect in a thin cavity. Photographs of steady flows with medicinal paraffin in a Hele-Shaw cell of depth 2·0 cm, length 30·0 cm, width 0·6 cm; heated strip of length 10 cm. Values of $10^{-4}A$: (*a*) 1·02, (*b*) 1·72, (*c*) 2·24, (*d*) 2·32, (*e*) 2·90, (*f*) 3·97, (*g*) 1·10 (HSI: 1–9).

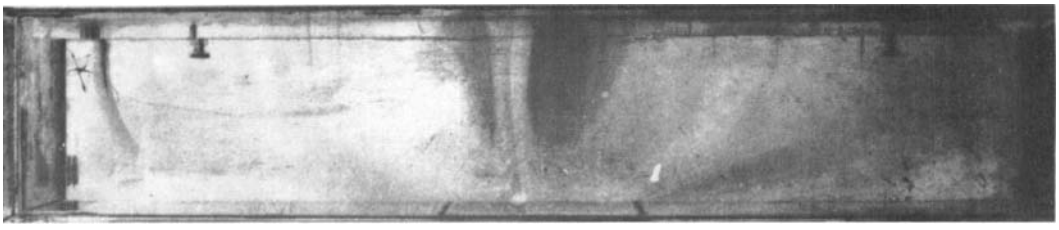

FIGURE 12. Natural discharge. Photograph of steady flow in a Hele-Shaw cell with: $H = L = 10$ cm, $E = 50$ cm, $b = 0{\cdot}318$ cm, at Rayleigh number $A = 420$. Compare with figure 10.